Research Article

Wejdan Al-Otaibi, Naser M. Alandis, and Manawwer Alam*

Leucaena leucocephala oil-based poly malate-amide nanocomposite coating material for anticorrosive applications

https://doi.org/10.1515/epoly-2023-0036
received April 27, 2023; accepted May 29, 2023

Abstract: This article describes the synthesis of polyesteramide (PEA) resin from *Leucaena leucocephala* oil (LLO) obtained from seeds of *L. leucocephala* tree, locally grown in King Saud University Campus. LLO was transformed into amide diol by based catalyzed amidation reaction, followed by esterification reaction with malic acid (MA), that resulted in LLO-based PEA (LPEA). The synthesis was performed without using any solvent or catalyst. Fourier-transformation infrared spectroscopy and nuclear magnetic resonance confirmed the formation of LPEA by the introduction of amide and ester moieties. LPEA was further reinforced with nano graphene oxide (GO) and fabricated into nanocomposite corrosion protective coatings (LPEA/GO). LPEA/GO coatings obtained were tough, flexibility retentive and showed good corrosion resistance performance toward 3.5 w/w% NaCl medium. Thermogravimetric analysis confirmed good thermal stability of coatings with safe usage up to 200°C.

Keywords: polyesteramide, coatings, graphene oxide, corrosion, thermal stability

1 Introduction

Plant crops and products are utilized as food crops, feed crops, ornamental crops, industrial crops, and others. The hazards and expenses associated with petro-based chemicals have motivated the researchers to substitute sustainable resource-based raw materials for the synthesis of monomers and polymers. In this context, the industrial crops are distinguished substitutes for petro-based chemicals. The industrial seed oils are rich in functional groups that can be transformed into monomers and polymers with applications as biodiesel, lubricants, inks, coatings, and paints. *Leucaena leucocephala* is an agro-industrial crop, belonging to the family Fabaceae (sub-family Mimossoideae). It has found bioenergetic applications in biodiesel, biogas, ethanol, char, activated carbon, and others, utilizing seeds, leaves, bark, wood, and legumes of the tree (1). *L. leucocephala* seed oil (LLO) is rich in linoleic, oleic, palmitic, and stearic acids, with the highest composition of linoleic acid (2,3).

Polyesteramide (PEA) resins contain both ester and amide functional groups in their backbone. They are transformed into corrosion-resistant, high-performance coatings. However, mostly they are synthesized at high temperatures, in the presence of solvents, in several steps, from synthetic diols and dicarboxylic acids (4). An alternate feasible method is to synthesize PEA from sustainable resource-based raw materials, i.e., a vegetable oil (VO)-derived diol and a naturally available dicarboxylic acid with the inclusion of a nanofiller for reinforcement, at lower temperatures without the use of any solvent (3,5).

Malic acid (MA) is obtained from fruits such as apples, guavas, grapes, and others. It is a dicarboxylic acid containing a hydroxyl group and used in flavorants, preservatives, cosmetics, medicines, and others (6–9).

Graphene oxide (GO) has been used as modifier component for coatings, toward corrosion protection of substrates such as mild steel, carbon steel, copper, aluminum, and others (10). GO, used as nanofiller (up to 0.5–1 wt%) in alkyd-based coatings, has dramatically improved the anticorrosion properties of nanocomposite coatings (11–13). GO-dispersed waterborne soy alkyd nanocomposite, synthesized through solventless approach, has shown superior corrosion protection performance compared to the plain soy alkyd coatings (11). Sunflower alkyd/GO coatings have shown high level of durability, superior physico-mechanical performance, and corrosion protection ability (12). GO-dispersed *Garcinia gummigutta* VO nanocomposite

*** Corresponding author: Manawwer Alam,** Department of Chemistry, College of Science, King Saud University, P.O. Box 2455, Riyadh 11451, Saudi Arabia, e-mail: malamiitd@gmail.com, maalam@ksu.edu.sa
Wejdan Al-Otaibi, Naser M. Alandis: Department of Chemistry, College of Science, King Saud University, P.O. Box 2455, Riyadh 11451, Saudi Arabia

coating on mild steel has shown efficient anticorrosion performance in 3.5 wt% NaCl medium, by the dispersion of 0.3 wt% GO (14).

This article describes the synthesis of PEA resin (LLO-based PEA; LPEA) from *Leucaena* oil amide diol (LOAD) and MA. The synthesized LPEA was reinforced with GO and developed into anticorrosive coatings for mild steel. The structure of LPEA was established by Fourier-transformation infrared spectroscopy (FTIR) and nuclear magnetic resonance (NMR) techniques and the interaction of GO with LPEA matrix was investigated by FTIR. The morphology of the synthesized resin was studied by scanning electron microscopy (SEM) and the thermal stability was assessed by thermogravimetric analysis (TGA).

The research work is focused on value-addition to a locally grown plant crop, by an environmentally safe and benign method, selecting sustainable resource-based monomers and opting for solventless synthesis strategy.

2 Materials

Diethanolamine (AppliChem GmbH, Darmstadt, Germany), MA (Scharlau, Chemie, Spain), sodium metal, sodium chloride (BDH Chemicals Ltd, Poole, England), toluene (Fisher Scientific Company, New Jersey, USA), diethyl ether, and methanol (Sigma-Aldrich, St. Louis, USA) were used as received. GO was obtained from Grafen Chemical Industries Co (Ankara, Turkey).

Seeds of *L. leucocephala* tree were collected from King Saud University campus in the month of March. *L. leucocephala* seed oil was extracted using Soxhlet apparatus as reported in our previously published article (3).

2.1 Synthesis of *N*,*N*-bis(2-hydroxyethyl) amide diol (LOAD)

LOAD was prepared according to our previously published article with LLO and sodium methoxide at 120°C (3,15).

2.2 Synthesis

2.2.1 LPEA

LOAD (0.08 mol) was placed in a four-necked flat-bottomed conical flask; the temperature was raised to 50°C with continuous agitation. MA (0.08 mol) was added in pinches slowly, under continuous stirring, to the flask containing LOAD, and after this addition was completed, the temperature was raised to 90°C. The contents were stirred, and this temperature was maintained until a clear and transparent resin was obtained, after which the heating was cut-off, the contents were allowed to cool to room temperature. The reaction was monitored by FTIR, by carefully observing the change in the absorption band for the hydroxyl group (3,370 cm^{-1}). The reaction was carried out without any solvent, and this required vigilant monitoring of viscosity changes during the course of reaction. The other pre-requisites of solvent-less synthesis were the optimization of reaction temperature as well as the amount of MA.

2.2.2 LPEA/GO nanocomposite

To the pre-determined amount of LPEA, GO was added in different weight percentages (0.25, 0.50, and 0.75%, w/w, on the weight of LPEA) and was dispersed in LPEA via a mechanical mixer (Dispers Master, Sheen Instruments Ltd, UK) at 30°C, mixed at 3,000 rpm for 2 h with to form LPEA/0.25GO, LPEA/0.50GO, and LPEA/0.75GO. The nanocomposites were placed undisturbed for 14 days to assure that no phase separation, agglomeration, or abnormal viscosity changes occurred (11).

2.3 Preparation of LPEA and LPEA/GO nanocomposite coatings

Before the application of coating material on the panels, surface preparation of the panels (composition: Fe, 99.51%; Mn, 0.34%; C, 0.10%; and P, 0.05%) of standard sizes was carried out for deburring and refinishing the panels with silicon carbide paper and degreasing with methanol and acetone. LPEA and LPEA/GO were diluted with 40% (w/w) toluene and were applied by brush on panels of standard sizes (70 mm × 25 mm × 1 mm) for the evaluation of their physico-mechanical performance, gloss measurements, and corrosion tests in 3.5% (w/w) NaCl medium. For SEM analysis, another set of circular panels (diameter 1 cm, thickness 150 μm) was prepared. To optimize the baking temperature and time, the coated panels were placed in hot air oven for different temperatures and time periods. The most adequate curing temperature and time were found as 150°C for 40 min (LPEA) and 140°C for 40 min (LPEA/GO).

3 Characterization

The structural elucidation of LPEA was carried out by FTIR (FTIR spectrophotometer; Spectrum 100, Perkin Elmer Cetus Instrument, Norwalk, CT, USA) and nuclear magnetic resonance (NMR) (^{1}H NMR and ^{13}C NMR; JEOL DPX400MHz, Japan) using deuterated chloroform and dimethyl sulfoxide as solvents and tetramethylsilane as internal standard. The matrix–GO interactions were investigated by FTIR. The dispersion of GO in LPEA was observed by SEM (JSM 7600F; JEOL) and transmission electron microscopy (TEM; JEM-2100F; JEOL). Thermal stability of LPEA and LPEA/GO was assessed by TGA and differential scanning calorimetry (DSC) (Mettler Toledo AG, Analytical CH-8603, Schwerzenbach, Switzerland), in N_2 atmosphere at the heating rate of 10°C·min^{-1}.

Thickness measurements (ASTM D 1186-B), physico-mechanical performance evaluation [scratch hardness (BS 3900), crosshatch (ASTM D3359-02), pencil hardness test (ASTM D3363-05), impact test (IS 101 part 5 s^{-1}, 1988), flexibility/bending test (ASTM D3281-84), gloss (gloss meter, Model: KSJ MG6-F1, KSJ Photoelectrical Instruments Co., Ltd., Quanzhou, China), and contact angle measurements (CAM200 Attention goniometer) were performed by standard methods.

For corrosion resistance test, an exposed surface area of 1.0 cm^2 was fixed by PortHoles electrochemical sample mask, with Pt electrode as counter electrode, and 3 M KCl filled silver electrode as reference electrode (Auto lab Potentiostat/galvanostat, PGSTAT204-FRA32, with NOVA 2.1.6 software; Metrohom Autolab B.V. Kanaalweg 29-G, 3526 KM, Utrecht, Switzerland), while the specimens were attended as working electrode.

4 Results and discussion

The synthesis of LPEA was carried out without any solvent and at reduced temperature compared to other VO-based PEA resins (4,16). In solvent-less synthesis, the reaction temperatures are reduced due to most favorable kinetics that allows for complete conversions, often without catalysis (17). The hydroxyl functional group of LOAD reacted with the carboxylic functional group of MA, by esterification reaction producing LPEA (Scheme 1). LPEA on dispersion of GO produced LPEA/GO nanocomposite. Both LPEA and LPEA/GO rendered mechanically strong and chemically resistant coatings.

LPEA and LPEA/GO resins were soluble in toluene, tetrahydrofuran, dimethylsulfoxide, 1,2-dichloroethane, furan, pyridine, cyclohexene, cyclohexane, and benzene; sparingly soluble in acetone, chloroform, methanol, 1-hexanol, methylbutanol, propanol, 1-4 dioxane, *n*-octane, ethanol, isoamyl alcohol, cyclohexane, ethanol, diethylether, and petroleum ether; and insoluble in distilled water and acetonitrile.

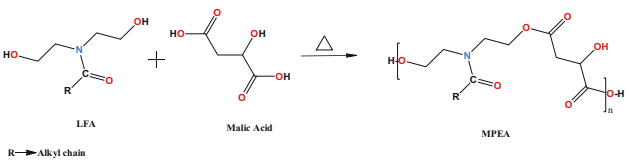

Scheme 1: Synthesis of LPEA.

4.1 Spectral analysis

FTIR (υ, cm^{-1}): Structure elucidation of LOAD by FTIR and NMR has been discussed in a previous manuscript (3). FTIR spectrum of LPEA (Figure 1) showed absorption bands at different wavenumber values typical for the constituent functional groups, present in VO-based PEA, i.e., –OH (str, broad at 3,346), –C═C–H (3,012), –CH_3, –CH_2 (str 2,854, 2,926),

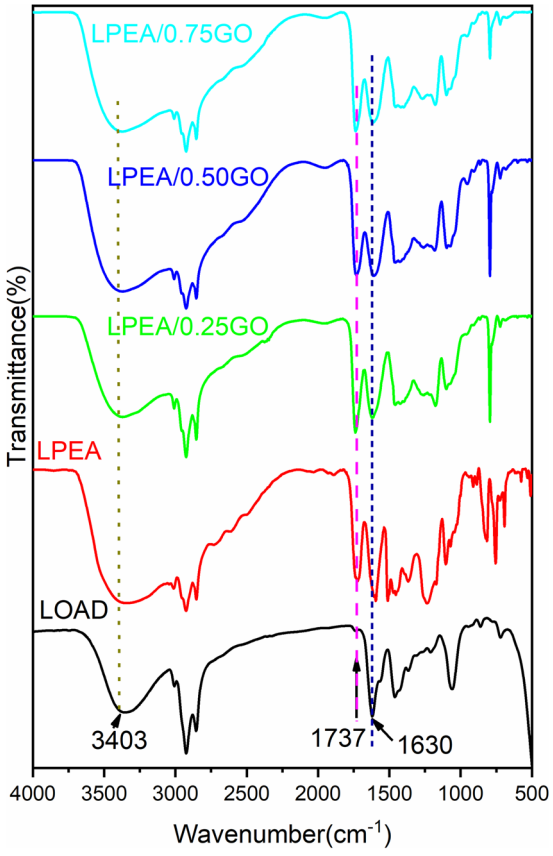

Figure 1: FTIR spectra of LPEA, LPEA/0.25GO, LPEA/0.5GO, and LPEA/0.75GO.

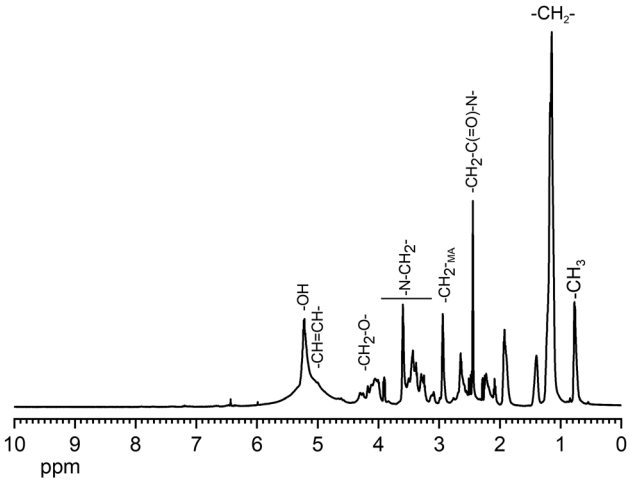

Figure 2: ^{1}H NMR spectrum of LPEA.

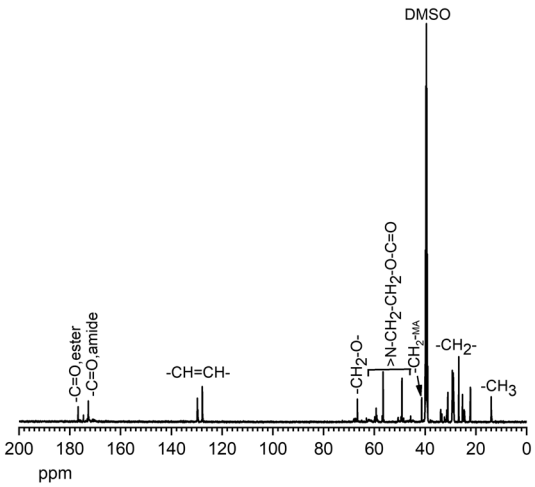

Figure 3: ^{13}C NMR spectrum of LPEA.

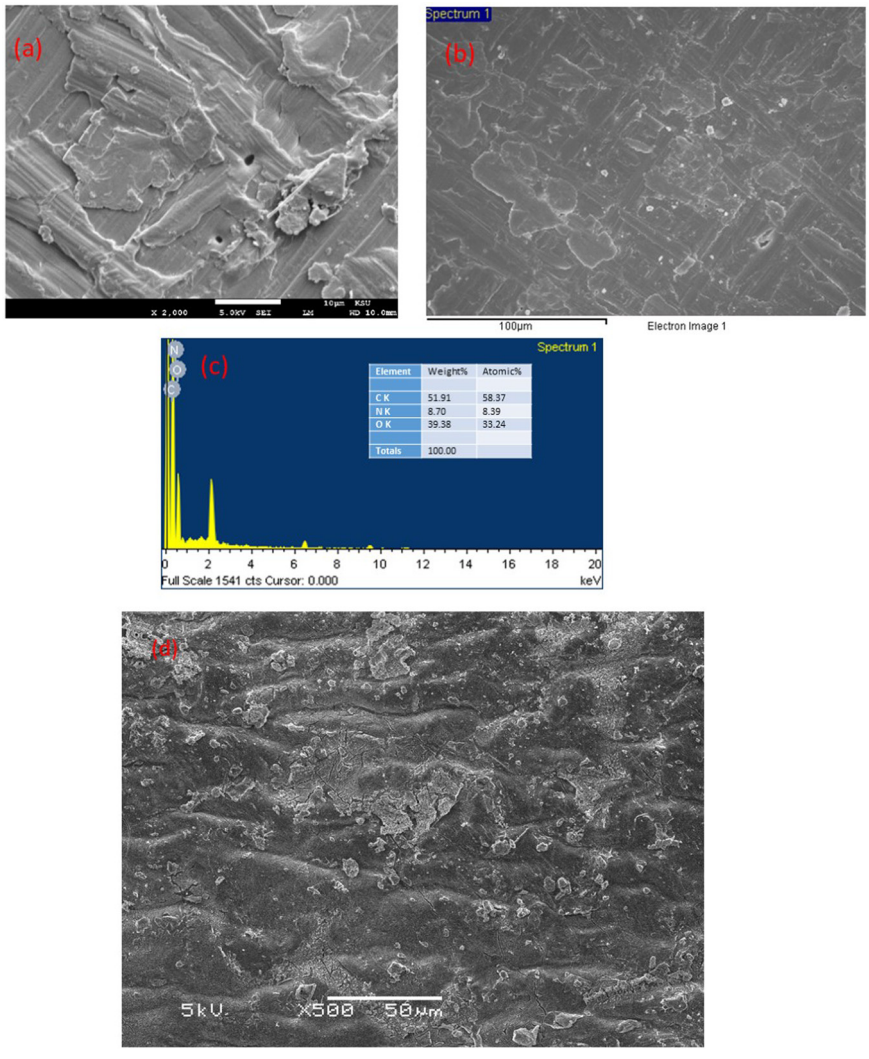

Figure 4: SEM image of GO (a), SEM image of LPEA/0.5GO (b), EDX graph of LPEA/0.5GO (c), and SEM image after 18 days immersion in 3.5% NaCl (d).

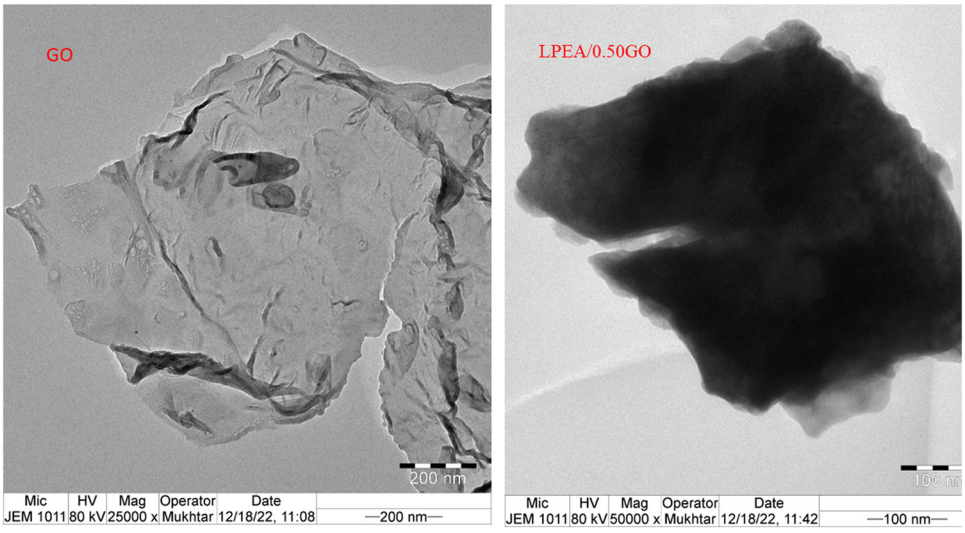

Figure 5: TEM image of GO (left) and LPEA/0.5GO (right).

Table 1: The physico-mechanical properties of LPEA/GO nanocomposite

Properties	LPEA	LPEA/ 0.25GO	LPEA/ 0.50GO	LPEA/ 0.75GO
Scratch hardness (kg)	1.8	2.1	2.4	2.4
Impact (680 g·m^{-1})	Pass	Pass	Pass	Pass
Bending (1/8″)	Pass	Pass	Pass	Pass
Pencil hardness	1H	2H	3H	3H
Cross hatch (%)	100	100	100	100
Gloss at 60°	86	90	97	94
Thickness (micron)	112	125	131	132

>C═O ester (str 1,721), >C═O amide (1,606), –CH_3, –CH_2 (bending, 1,470–1,455), –(C$_в$O) –O–C (str, 1,235–1,103), –C–O–H (–C–O str, 1,070), –O–H (bending, 801–928). The absorption band for hydroxyl occurred as a broad band due to hydrogen bonding. LPEA/GO also exhibited the presence of these absorption bands. The inclusion of GO could be discerned not by the presence of the absorption bands of GO (since GO has large number of –O containing functional groups that tend to overlap with functional groups of LPEA), but with shift in absorption values in case of –OH (3,371–3,373), >C═O ester (str 1,728–1,738), >C═O amide (1,611–1,620), relative to those in LPEA, due to interactions between LPEA and GO (18–20).

^{1}H NMR (DMSO-d$_6$, δ, ppm) LPEA: 5.23 (–O**H**), 5.20 (–C**H**═C**H**–), 4.02–4.12 (–C**H**$_2$–O–C(═O)–), 3.55–3.60 (–N–C**H**$_2$–CH$_2$–O–C(═O)–, 3.40–3.43 (–N–CH$_2$–C**H**$_2$–O–C(═O)–), 2.64–2.94 (–C**H**$_{2-MA}$) 2.26–2.51 (–C**H**$_2$–C(═O)–N–), 1.14–2.10 (–C**H**$_2$–), 0.76–0.77 (–C**H**$_3$) (Figure 2).

^{13}C NMR (DMSO-d$_6$, δ, ppm): 176.76 (>**C**═O$_{ester}$), 172.73–174.65 (>**C**═O$_{amide}$), 129.60–129.72 (–**C**H═**C**H–), 66.65 (–CH$_2$–O–), 59.02–49.12 (>N–**C**H$_2$**C**H$_2$–O–C(в)O–), 41.37 (–**C**H$_{2-MA}$), 22.14–33.90 (**C**H$_{2chain}$), 13.96 (–**C**H$_3$) (Figure 3).

The spectral analysis confirmed the reaction of LOAD and MA forming LPEA.

4.2 Morphology

SEM micrograph (Figure 4a) of GO showed wrinkled sheet-like structure due to exfoliation and restacking, as reported previously (11,18,19). The nanocomposite morphology has been given in Figure 4b. SEM micrograph showed the presence of GO sheets in the matrix. LPEA/0.05GO nanocomposite showed

Figure 6: Contact angle of LPEA (a) and LPEA/0.5GO (b).

Table 2: The electrochemical impedance (EIS) parameter for LPEA/0.50GO coating under 3.5 wt% NaCl solution at room temperature

Immersion (day)	Rs (Ω·cm^2)	Rc (MΩ·cm^2)	CPE		OCP (V)	χ^2
			Y_0, nMho·s^n	n		
1	645	1.22	1.26	0.904	0.163	0.14
3	643	1.40	1.43	0.874	0.155	0.05
6	638	1.46	1.58	0.865	0.130	0.08
9	637	1.44	1.59	0.865	0.120	0.24
12	635	1.26	1.68	0.855	0.100	0.18
15	578	2.93	2.01	0.854	0.075	0.30
18	554	2.62	2.63	0.835	0.036	0.57

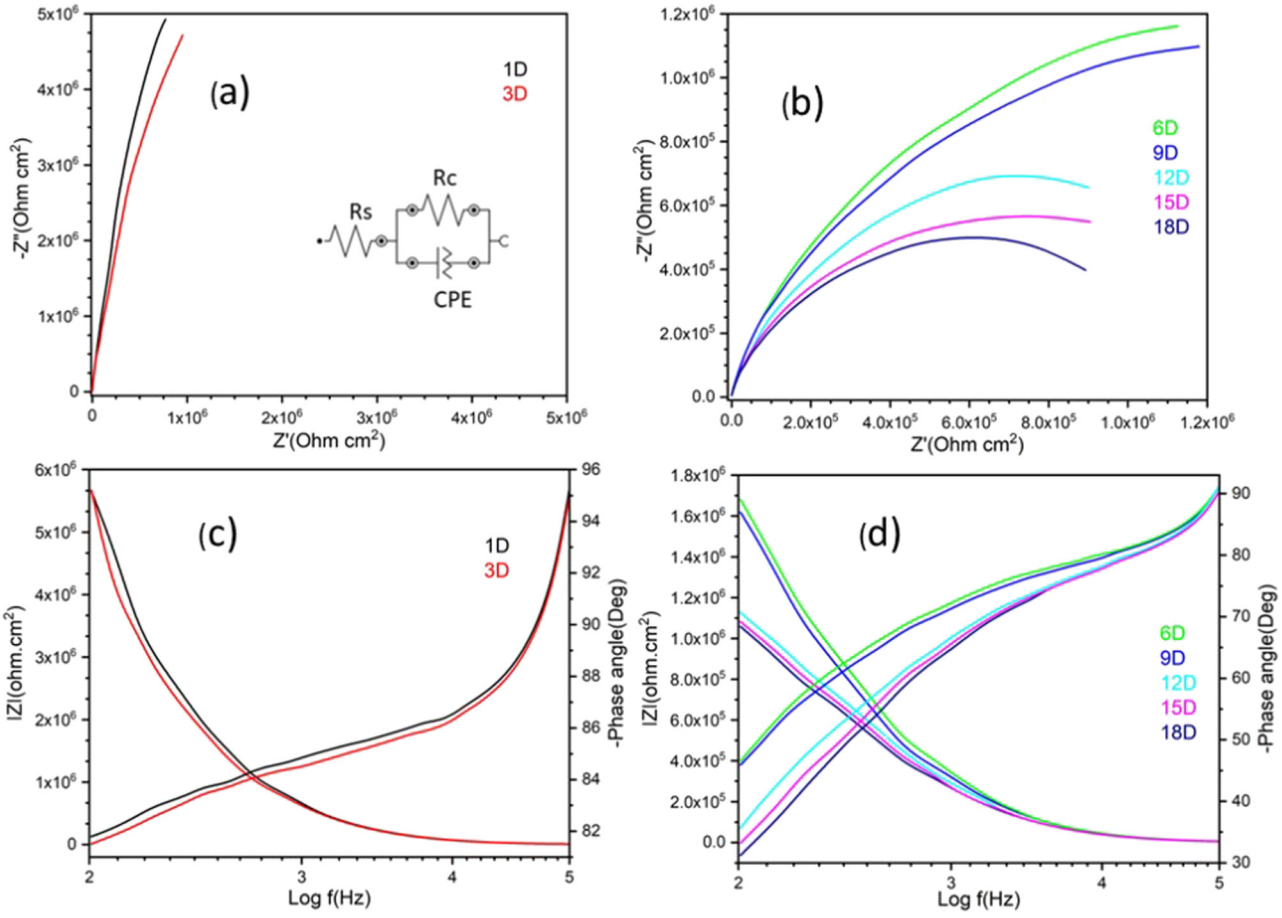

Figure 7: EIS (a and b) and Bodetheta (c and d) spectra of LPEA/0.5GO.

non-uniform, crumpled surface as a result of dispersion of GO. However, no pin-holes or cracks were evident. EDX (Figure 4c) peaks due to C (58.31%), N (8.39%), and O (33.24%) were evident and confirmed the presence of GO in LPEA nanocomposite.

TEM image of GO (Figure 5) showed crumpled edges and, in some regions, sharp edges were evident. The dark regions were also visible for the piles of GO sheets. LPEA/0.5GO showed dark contrast, due to the LPEA layer covering the GO sheets.

4.3 Coating properties

4.3.1 Physico-mechanical properties

The coatings were prepared at temperature 140–150°C for 40 min; the nanocomposite coatings showed lower drying temperature compared to the plain LPEA coatings. The coatings obtained were tough and glossy with uniform

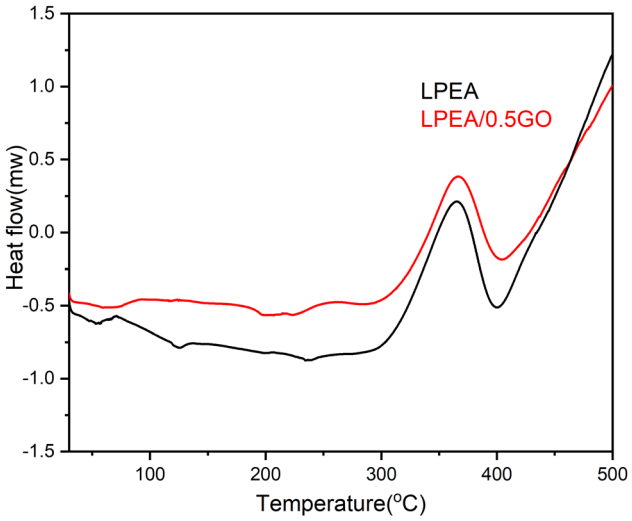

Figure 8: DSC thermogram of LPEA and LPEA/0.5GO.

thickness: 112 µm (LPEA) and 125–132 µm (LPEA/GO). The coatings showed good scratch hardness and pencil hardness that increased from LPEA, LPEA/0.25GO to LPEA/0.50GO, remained unaffected up to 0.50 wt% inclusion of GO, and showed deterioration after >0.75 wt% loading of GO. The cross-hatch test, impact resistance, and bend test performance results of coatings were not affected by the inclusion of GO (Table 1). However, at higher loading of GO, these characteristics displayed a deteriorating trend. At higher amount of GO, agglomerates were formed, and viscosity increased abnormally and deteriorated the overall performance of coatings.

The contact angle measurements (Figure 6) showed that the contact angle increased from 71° in LPEA to 78° in LPEA/GO. This indicated a slight improvement in hydrophobicity after the inclusion of GO, which also supported better corrosion protection performance of the nanocomposite coating.

4.3.2 Corrosion resistance performance – electrochemical studies (EIS)

For LPEA/0.5GO, Nyquist plots were obtained for various immersion times (1, 3, 6, 9, 12, 15, and 18 days) in 3.5 wt% NaCl solution. These plots displayed Rs, electrolyte resistance; Cc, coating capacitance; and Rc, coating resistance. As evident (Table 2), with an increase in the number of days of immersion of coated panels in the saline medium, Rs is decreased (645–554 $\Omega \cdot cm^2$) while Rc is increased (1.22–2.62 $M\Omega \cdot cm^2$), as a consequence of coating surface impairment. As the coated panels spend more time in a corrosive saline medium, their surface becomes weaker with ease of diffusion by corrosive ions. In the case of coatings that are not corrosion resistant, a sharp decrease in Rs might be witnessed with the passage of time; however, in the present case, a sluggish decrease is observed. Rs reached its least value after 18 days of exposure. GO provided barrier protection against the diffusion of corrosive ions and prevented the corrosive ions to reach the metal surface and deteriorate it. Coating performance also depended upon the distribution of GO sheets in matrix and their method of dispersion (21). Figure 7 shows that the impedance value decreased as the days of immersion in the medium increased. The phase angle value for 1-day immersion was 95°, decreased to 90° for 6-day immersion,

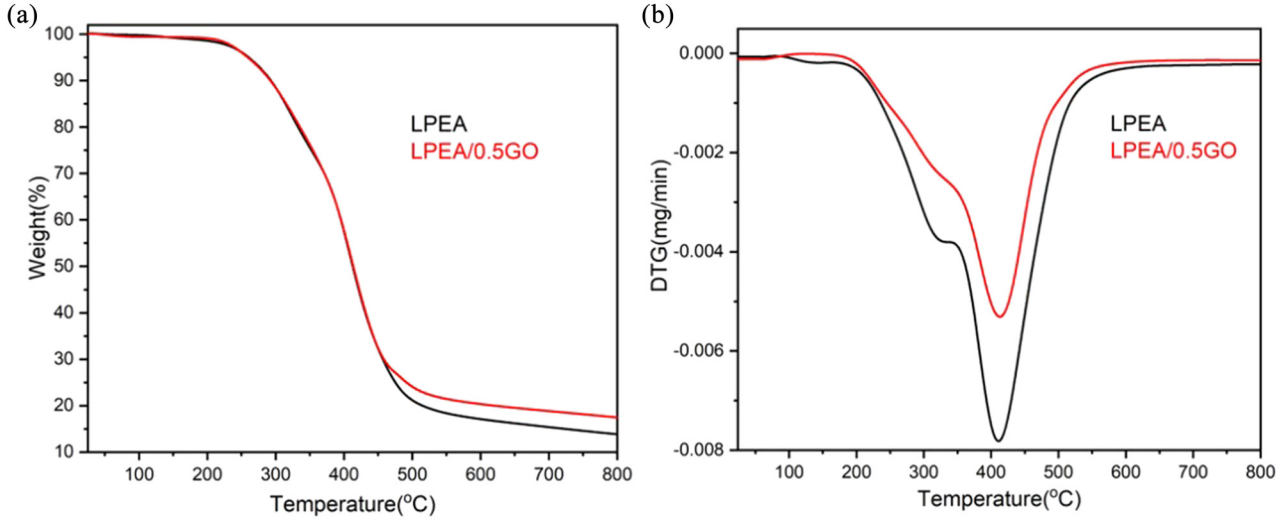

Figure 9: TGA (a) and DTG (b) thermograms of LPEA and LPEA/0.5GO.

and remained unaffected at 90° even up to 18-day immersion. Thus, the pronounced deterioration occurred up to 6 days of exposure to the corrosive media.

The coated panel of LPEA/0.5GO was immersed in 3.5 wt% NaCl and was subjected to SEM analysis (Figure 4d). The panel was found to be unaffected after immersion in the medium for 18 days. The salt deposition was evident on the panel surface while there were no cracks and no pore formation visible under SEM.

4.4 TGA

DSC thermogram (Figure 8) of LPEA and LPEA/0.50GO showed an endotherm from 365 to 475°C, respectively, followed by an exothermic event. TGA thermogram (Figure 9a) of LPEA showed two steps and LPEA/0.50GO depicted somewhat a single-step degradation pattern, which is also evident in the DTG thermogram (Figure 9b). 5 wt% loss had occurred until 258°C while the rest 75 wt% decomposition had occurred until 474°C (LPEA) and 490°C (LPEA/0.50GO). Among the nanocomposites, LPEA/0.50GO showed higher thermal stability, compared to LPEA, while at 0.75 wt% inclusion of GO, it had deteriorated. This conformed with the fact that higher inclusion of GO leads to impaired physico-mechanical properties, reduced gloss, and lowered thermal stability. Thus, improved thermal stability could be achieved until the dispersion of 0.50 wt% GO in LPEA/0.50GO, due to fine dispersion of GO and good interaction with the matrix (11). Beyond >0.50 wt%, the excess GO caused agglomeration and the thermal stability deteriorated (20).

5 Conclusion

This article described the synthesis of *L. leucocephala* oil-based poly malate-amide/GO nanocomposite coating material. The synthesis was carried out without any organic solvent, which resulted in reduced reaction temperature without catalysis. The coatings obtained were flexible, scratch resistant, impact resistant, and thermally stable, with the dispersion of GO up to 0.5 wt% loading of GO. Above 0.75 wt% inclusion of GO, the coatings lost their integrity and homogeneity, and overall performance was impaired. The coatings showed good corrosion protection performance in the saline medium. The approach is simple and environmentally safe and provides a value-addition pathway for a locally available plant crop.

Acknowledgments: The authors extend their appreciation to the Deputyship for Research and Innovation, "Ministry of Education" in Saudi Arabia for funding this research (IFKSUOR3-538-1).

Author contributions: Wejdan Al-Otaibi: methodology, data generation, drafting; Naser M. Alandis: formal analysis, project administration; Manawwer Alam: formal analysis, writing – review and editing, manuscript handling.

Conflict of interest: The authors state no conflict of interest.

References

(1) Alemán-Ramirez JL, Okoye PU, Torres-Arellano S, Mejía-Lopez M, Sebastian PJ. A review on bioenergetic applications of *Leucaena leucocephala*. Ind Crop Prod. 2022;182:114847.
(2) Nehdi IA, Sbihi H, Tan CP, Al-Resayes SI. *Leucaena leucocephala* (Lam.) de Wit seed oil: Characterization and uses. Ind Crop Prod. 2014;52:582–7.
(3) Alam M, M Alandis N, Sharmin E, Ahmad N, Husain FM, Khan A. Mechanically strong, hydrophobic, antimicrobial, and corrosion protective polyesteramide nanocomposite coatings from *Leucaena leucocephala* oil: A sustainable resource. ACS Omega. 2020;5(47):30383–94.
(4) Alam M, Akram D, Sharmin E, Zafar F, Ahmad S. Vegetable oil based eco-friendly coating materials: A review article. Arab J Chem. 2014;7(4):469–79.
(5) Alam M, Ahmed M, Altaf M, Husain FM. Rapeseed oil-based hippurate amide nanocomposite coating material for anticorrosive and antibacterial applications. Open Chem. 2022;20(1):725–35.
(6) Gadang VP, Hettiarachchy NS, Johnson MG, Owens C. Evaluation of antibacterial activity of whey protein isolate coating incorporated with nisin, grape seed extract, malic acid, and EDTA on a Turkey frankfurter system. J Food Sci. 2008;73(8):M389–94.
(7) Manickaraj SSM, Pandiyarajan S, Liao AH, Lai KL, Ramachandran A, Lee KY, et al. Malic acid pathway of constructing high-performance Ni anticorrosive coatings using supercritical-CO_2 electrodeposition. Mater Sci Semicond Process. 2022;148:106780.
(8) Shahruzzaman MD, Islam MS, Haque MM, Hossain MS, Bakr MA. Malic acid butane-1, 4-diol-glycerol co-polyester as an enteric coating material. Int J Sci Eng Res. 2015;6:1460–3.
(9) Zhang J, Huang J, Zhu G, Yu X, Cheng J, Liu Z, et al. Self-healing, recyclable, and removable UV-curable coatings derived from tung oil and malic acid. Green Chem. 2021;23(16):5875–86.
(10) Ollik K, Lieder M. Review of the application of graphene-based coatings as anticorrosion layers. Coatings. 2020;10(9):883.
(11) Irfan M, Bhat SI, Ahmad S. Reduced graphene oxide reinforced waterborne soy alkyd nanocomposites: Formulation, characterization, and corrosion inhibition analysis. ACS Sustain Chem Eng. 2018;6(11):14820–30.

(12) Selim MS, El-Safty SA, Shenashen MA, El-Sockary MA, Elenien OMA, El-Saeed AM. Robust alkyd/exfoliated graphene oxide nanocomposite a surf coat. Prog Org Coat. 2019;126:106–18.
(13) Zhu K, li X, Wang H, Li J, Fei G. Electrochemical and anti-corrosion behaviors of water dispersible graphene/acrylic modified alkyd resin latex composites coated carbon steel. J Appl Polym Sci. 2017;134(11):44445.
(14) Hegde MB, Nayak SR, Mohana KNS, Swamy NK. *Garcinia gummi-gutta* vegetable oil–graphene oxide nano-composite: An efficient and eco-friendly material for corrosion prevention of mild steel in saline medium. J Polym Environ. 2020;28(2):483–99.
(15) Alam M, Alandis NM. Corn oil based poly(ether amide urethane) coating material—synthesis, characterization and coating properties. Ind Crop Products. 2014;57:17–28.
(16) Ahmad S, Ashraf SM, Zafar F. Development of linseed oil based polyesteramide without organic solvent at lower temperature. J Appl Polym Sci. 2007;104(2):1143–8.
(17) Kaupp G. Solvent-less organic synthesis. Kirk-Othmer encyclopedia of chemical technology. Weinheim, Germany: Wiley-VCH; 2012. p. 1–43. https://doi.org/10.1002/0471238961.solvkaup.a01.
(18) Aliyev E, Filiz V, Khan MM, Lee YJ, Abetz C, Abetz V. Structural characterization of graphene oxide: Surface functional groups and fractionated oxidative debris. Nanomaterials. 2019;9(8):1180.
(19) Choi YJ, Kim E, Han J, Kim JH, Gurunathan S. A novel biomolecule-mediated reduction of graphene oxide: A multifunctional anti-cancer agent. Molecules. 2016 Mar 18;21(3):375.
(20) Li L, Li X, Shen Y, Chen X, Jiang L. Hydrophobicity and corrosion resistance of waterborne fluorinated acrylate/silica nanocomposite coatings. e-Polymers. 2021;21(1):779–92.
(21) Pourhashem S, Vaezi MR, Rashidi A, Bagherzadeh MR. Exploring corrosion protection properties of solvent based epoxy-graphene oxide nanocomposite coatings on mild steel. Corros Sci. 2017;115:78–92.